INTERNATIONAL JOURNAL OF AGRICULTURE & BIOLOGY
ISSN Print: 1560–8530; ISSN Online: 1814–9596
25–880/2026/35:350211
http://www.fspublishers.org

Full Length Article

From Pixels to Precision: Smartphone-based Deep Learning for Scalable Nitrogen Assessment in Maize

Rabia Zafar[1,2*], Muhammad Shahid Farid[1], Muhammad Hassan Khan[1] and Rashid Mehmood[3]
[1]*Department of Computer Science, University of the Punjab, Lahore 54590, Pakistan*
[2]*Department of Computer Science and Engineering, University of Engineering and Technology, Narowal Campus, Pakistan*
[3]*Department of Soil Science, University of the Punjab, Lahore 54590, Pakistan*
[*]For correspondence: rabia.zafar@uet.edu.pk
Received 22 August 2025; Accepted 06 November 2025; Published online 13 December 2025

Editor: Mubshar Hussain

Abstract

Nitrogen deficiency remains one of the most critical constraints to sustain maize productivity. While conventional measurement techniques are destructive, costly, and labor-intensive; therefore, a non-destructive, smartphone-based framework that integrates automated leaf segmentation using a deep learning model (U²-Net) with color-metric analysis to estimate nitrogen content directly from field-acquired images is developed. The model was trained and evaluated on a comprehensive dataset of 1,188 maize (*Zea mays* L.) leaf samples from 11 varieties, cultivated under varying nitrogen treatments and photographed using multiple smartphones. Estimation results showed a significant correlation with both laboratory Kjeldahl digestion benchmarks and Greenseeker normalized difference vegetation index (NDVI) readings. Collective and variety-specific evaluations demonstrated strong agreement with reference measurements, with correlations reaching $\rho = 0.65$ overall and up to $\rho = 0.95$ at the variety level. Among the 26 tested color indices, $\frac{B}{R+G+B}$, $R-G$ and $G-B$ consistently emerged as the most reliable predictors of leaf nitrogen. Statistical testing using PERMANOVA further revealed that camera resolution significantly influences several color metrics, emphasizing the importance of device-aware calibration in practical deployments. This study demonstrates the potential of smartphones as scalable tools for nitrogen monitoring by combining accessibility, accuracy, and reproducibility, and also contributes an open dataset to support future research in digital agriculture. Future model iterations will aim to improve robustness to challenging field variables like extreme illumination, shadows, other camera resolutions and diverse leaf orientations, along with investigation of applicability with other cereal crops.

Keywords: Crop nitrogen estimation; Image processing; Leaf color analysis; Deep learning; Smartphone based sensing

Introduction

Optimizing plant growth through precise fertilization is critical for maximizing yield and maintaining crop quality (Ghazal *et al*. 2024). Inefficient fertilizer application, however, can lead to economic losses, environmental degradation, and suboptimal productivity (Taheri *et al.* 2021). Conventional nutrient assessment techniques, while reliable, are often destructive, laborious, and costly, underscoring the need for scalable and affordable alternatives (Haider *et al*. 2021). Advances in image-based plant phenotyping have created new opportunities for non-destructive monitoring of crop health, with applications such as improved fertilization strategies, frameworks for assessing soil fertility (Gürbüz and Kardeş 2024) and methods for evaluating cultivar-specific nitrogen (N) fixation (Altuntaş *et al*. 2024). A survey by Kamilaris and Prenafeta-Boldú in 2018 demonstrates that image-driven approaches, coupled with computational techniques, can achieve high precision in monitoring plant traits. Furthermore, integration with remote sensing expands their scalability for large-scale agricultural monitoring (Colorado *et al*. 2020; Lu *et al*. 2020).

Nitrogen is particularly important due to its central role in amino acid synthesis, nucleic acid formation and chlorophyll production. It directly influences photosynthesis and crop biomass (Govindasamy *et al*. 2023). Despite its significance, only about half of the applied N is effectively utilized by crops, with the remainder lost through denitrification, leaching, runoff, and volatilization. These inefficiencies reduce N use efficiency (NUE), elevate production costs, and contribute to environmental contamination (Yokamo *et al*. 2023). Monitoring N status with greater accuracy and frequency is therefore vital for

To cite this paper: Zafar R, MS Farid, MH Khan, R Mehmood (2026). From pixels to precision: smartphone-based deep learning for scalable nitrogen assessment in maize. *Intl J Agric Biol* 35:350211. https://doi.org/10.17957/IJAB/15.2441

sustainable crop management, improved NUE, and food security (Rawal *et al*. 2022; Govindasamy *et al*. 2023).

The estimation of N content in crops using consumer-grade visible light (Red, Green, Blue (RGB)) smartphone cameras and color indices, operating at both canopy and leaf scales is performed in studies *i.e*., (Amaral *et al*. 2018; Chen *et al*. 2022; Sánchez-Sastre *et al*. 2020; Yang *et al*. 2022). While satellite imagery offers a canopy-level perspective, its utility is frequently constrained by atmospheric conditions, temporal resolution limitations, and the expense of detailed imagery. At the leaf level, conventional cameras have been employed in various studies (Adhikari *et al*. 2020; Chen *et al*. 2020; Haider *et al*. 2021). However, most of these works were conducted under controlled lighting, experimental settings and environmental conditions, limiting their applicability in real-world field scenarios characterized by variable illumination, complex backgrounds, and diverse growth stages.

This study establishes a scalable, image-based framework for estimating N content in maize as it is a global staple whose productivity is intensely sensitive to N availability, making it an agronomically vital test subject. Furthermore, the plant itself offered a practical advantage; its large leaf and simple structure facilitate the study. This proposed method introduces a novel pipeline that integrates automated leaf segmentation *via* U²-Net with colorimetric analysis. It effectively eliminates background bias and enables accurate N analysis of 11 maize varieties from three smartphone resolutions, explicitly quantifying the model's robustness to genetic and hardware variations. Notably, this study also addresses a key research gap in plant phenotyping: the effect of varying camera resolutions on color-based metrics. Furthermore, a key contribution of this work is the creation and public release of a large, annotated dataset comprising 1,188 leaf samples with corresponding Kjeldahl and Greenseeker measurements, which provides a validated benchmark for future research. This work directly addresses the gap between laboratory-based measurement and in-field decision support by delivering a practical, cost-effective tool and a critical resource for the community.

Material and Methods

Data acquisition

In this study, eleven maize varieties (CIMMYT PAK, Agaiti-72, Pop-1, Sweet-1, YH-1898, FH-1046, Akbar, YH-548, Sahiwal Gold, YH-5427 and Gohar-19) grown at the research farm of the Department of Soil Science, Faculty of Agricultural Sciences, University of the Punjab, Lahore (31.493194° N, 74.297900° E) during Spring 2022. The experimental soil was classified as clay loam, with an electrical conductivity of 1.2 dS m^{-1}, a pH of 7.0, 0.74% organic matter, 0.04% total nitrogen, 10 mg. kg^{-1} available phosphorus and 160 mg. kg^{-1} extractable potassium. The experiment followed a factorial randomized complete block design (RCBD) with three replications. The first factor consisted of eleven maize cultivars: CIMMYT PAK, Agaiti-72, Pop-1, Sweet-1, YH-1898, FH-1046, Akbar, YH-548, Sahiwal Gold, YH-5427 and Gohar-19. Each cultivar was grown under four nitrogen levels (second factor), corresponding to 0%, 50%, 100% and 200% of the recommended nitrogen dose (227 kg N ha^{-1} for F_1 hybrids and 198 kg N ha^{-1} for open-pollinated varieties). Standard and uniform agronomic practices were maintained across all treatments.

Emphasizing practical field applicability, images were acquired using readily available equipment. A dark cardboard frame with a central window was used to standardize the imaging area, and leaf images were captured directly in the field using a smartphone camera. Three separate datasets were compiled using different smartphone cameras: an 8 MP Samsung device (Dataset I), a 10 MP device (Dataset II), and a 13 MP device (Dataset III). Each dataset contains 396 JPEG (Joint Photographic Experts Group) images (11 varieties × 4 treatments × 3 replicates × 3 images), resulting in a total of 1,188 images. The composition of the dataset is summarized in Table 1, with representative samples provided in Fig. 1.

Proposed methodology

This study establishes an image-based pipeline for estimating maize leaf N content by analyzing color features. A two-step preprocessing procedure (Fig. 2) was developed to extract standardized, clean images of the leaf lamina.

Image preprocessing and leaf segmentation

The initial step isolates the leaf from the cardboard background used during imaging. Several segmentation methods were evaluated, including color thresholding (Kulkarni 2012), multilevel thresholding, watershed segmentation (Shafarenko *et al*. 1997) and the deep learning models U²-Net (Qin *et al*. 2020) and Semantic Image Matting (Sun *et al*. 2021). U²-Net yielded superior results. The U²-Net architecture (Fig. 3) is particularly well-suited for this segmentation task due to its dedicated design for salient object detection (SOD), which enables effective training from scratch without dependence on pre-trained classification backbones. Its principal innovation lies in a two-level nested U-structure built using Residual U-Blocks (RUBs). Each RUB acts as an internal encoder-decoder, capturing multi-scale features within a single stage while maintaining feature map resolution. This design is enhanced by skip connections that propagate high-resolution spatial details, facilitating precise output reconstruction. The full network processes input images through a symmetric encoder-decoder pathway; the encoder downsamples and expands feature channels, while the decoder upsamples and reduces channels, seamlessly integrating multi-level features *via* skip connections. This results in a deep yet computationally efficient architecture capable of high-precision segmentation (Fig. 4).

Table 1: Comprehensive dataset description by image capturing device, including sample counts, resolution and treatment replication

Datasets	Samples	Treatments	Replicates	Resolution	Format	Images
Dataset-I	132	4	3	8 MP	JPEG	396
Dataset-II	132	4	3	10 MP	JPEG	396
Dataset-III	132	4	3	13 MP	JPEG	396

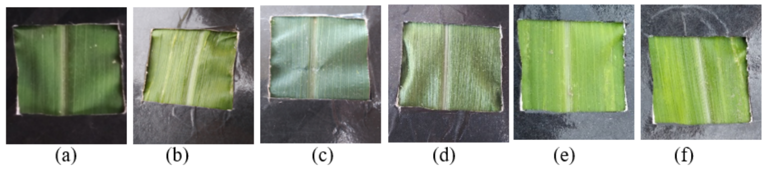

Fig. 1: Sample leaf images from datasets captured by three different smartphones. (**a-b**) Dataset I (8 MP), (**c-d**) Dataset II (10 MP) and (**e-f**) Dataset III (13 MP)

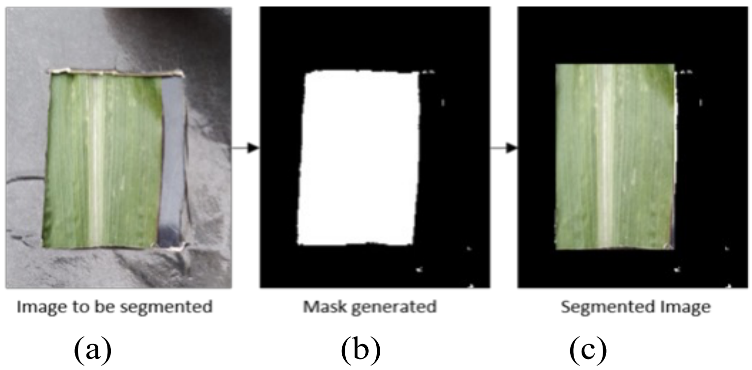

Fig. 2: Automated leaf segmentation pipeline. The process illustrates the sequential conversion of (**a**) an original field-acquired image to (**b**) a binary mask and finally to (**c**) an isolated leaf segment, effectively separating the target leaf from its complex background

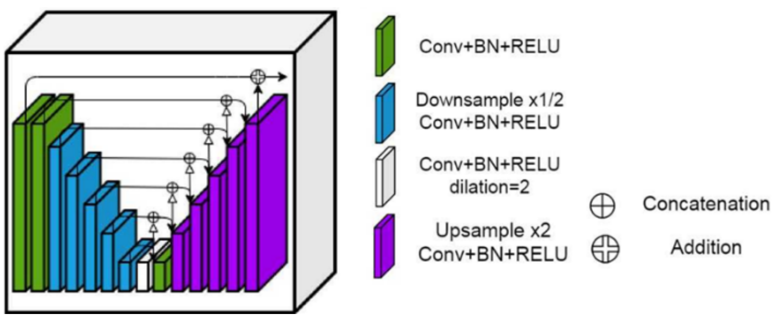

Fig. 3: Core architecture of the segmentation model, the Residual U-block (RSU). As introduced by Qin *et al*. (2020), this module was integral to our network for its ability to efficiently learn multi-scale feature representations from input images

While the pre-trained U^2-Net model performed well (Fig. 5), it occasionally misclassified the cardboard frame or fingers as foreground. To address this, the model was fine-tuned *via* transfer learning on an annotated subset from Dataset-III. The pre-trained model is used as foundation, now it can distinguish between badly trimmed cardboard edges in the background and foreground leaves that resemble human fingers. This optimized model, designated LeafDetectionU^{2}Net, achieved robust segmentation by learning to distinguish leaves from these specific artifacts.

Later, the segmentation mask from Leaf Detection U^2 Net was used to fit a minimum area bounding rectangle. This rectangle was rotated to correct skew and then cropped from the original image with a 10-pixel margin added to each side to eliminate any residual edge noise (Table 1).

Color metric extraction for N assessment

A suite of 26 color metrics was derived from preprocessed RGB imagery to assess their correlation with N content. An initial set of 18 metrics (M_1–M_{18}; Table 2), comprising simple RGB ratios, was adopted from established literature. For systematic reference, each metric was assigned a unique identifier using "M" to denote "Metric" with numerical subscripts ranging from 1 to 18 as detailed in Table 2.

Table 2: Comprehensive list of evaluated color-based vegetation indices for leaf nitrogen estimation. The table provides the unique identifier, and corresponding mathematical formula for each of the 18 preliminary metrics (M_1-M_{18})

Metric	Description	Metric	Description
M_1	R: average red component (Amaral *et al.* 2018)	M_{10}	$\frac{(R-G)}{(R+G)}$ (Yang *et al.* 2008)
M_2	G: average green component (Agarwal and Gupta 2018)	M_{11}	$\frac{(R-B)}{(R+B)}$ (Kawashima and Nakatani 1998)
M_3	B: average blue component	M_{12}	$\frac{(G-B)}{(G+B)}$
M_4	$\frac{R}{R+G+B}$	M_{13}	$\frac{(R-G)}{(R+G+B)}$ (Sánchez-Sastre *et al.* 2020)
M_5	$\frac{G}{R+G+B}$	M_{14}	$\frac{(R-B)}{(R+G+B)}$
M_6	$\frac{B}{R+G+B}$	M_{15}	$\frac{(G-B)}{(R+G+B)}$
M_7	$\mathbf{R-G}$ (Agarwal and Gupta 2018)	M_{16}	$\frac{2R(G-B)}{(G+B)}$ (Amaral *et al.* 2018)
M_8	$\mathbf{R-B}$ (Agarwal and Gupta 2018)	M_{17}	$\frac{2G(R-B)}{(R+B)}$
M_9	$\mathbf{G-B}$ (Agarwal and Gupta 2018)	M_{18}	$\frac{2B(G-B)/(G+B)}{(R+B)}$

For systematic reference, each metric was assigned a unique identifier using "M" to denote "Metric" with numerical subscripts ranging from 1 to 18

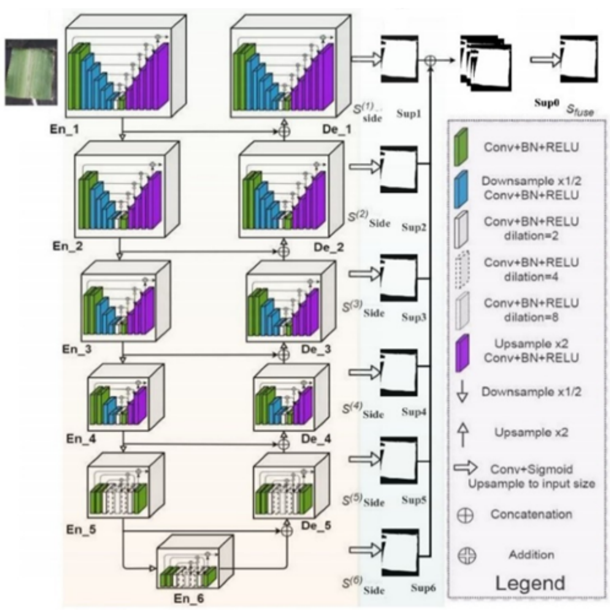

Fig. 4: Schematic of the U²-Net architecture (Qin *et al.* 2020) used for leaf segmentation. The model is a two-level nested U-structure that leverages Residual U-Blocks (RSUs) to capture contextual information at various scales, enabling robust salient object detection from complex backgrounds

A subsequent set of eight metrics (I_{M1}–I_{M4} for each of two indices) was formulated based on the methodology of Pagola *et al.* (2009). This approach combines two greenness indices, the I_{kaw} (Kawashima and Nakatani 1998) (Eq. 1) and I_{pca} (derived *via* PCA; Eq. 2), with four distinct aggregation techniques. The aggregation methods include: the arithmetic mean of RGB channel values (I_{M1}, Eq. 3), the arithmetic mean of the index value across the image (I_{M2}, Eq. 4) and two segmentation-based methods that cluster pixels by color similarity before computing a weighted mean (I_{M3}, Eq. 5; I_{M4}, Eq. 6).

$$I_{kaw} = \frac{R-B}{R+B} \tag{1}$$

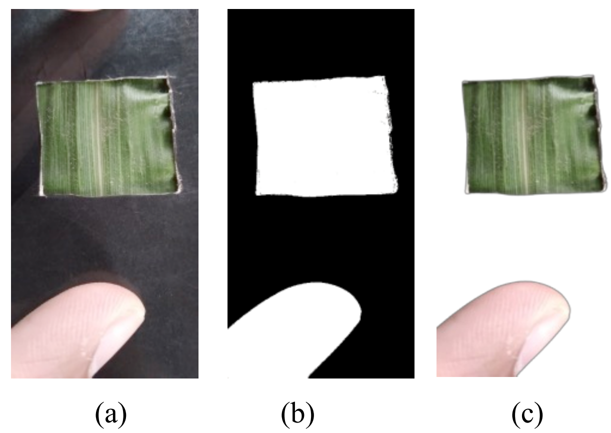

Fig. 5: U²Net pre-trained model segmentation results for an image containing a human thumb. (**a**) Sample image with a human thumb, (**b**) Segmentation Mask generated by U²Net and (**c**) background subtraction resulted by generated segmentation

$$I_{pca} = 0.6414|G-B| - 0.1168|R\ G| + 0.7582|R-B| \tag{2}$$

I_{M1}: the following is the basic aggregation of each color given by Eq. 3.

$$\bar{R} = \frac{1}{rc\sum R(i,j)}, \bar{G} = \frac{1}{rc\sum G(i,j)}, \bar{B} = \frac{1}{rc\sum B(i,j)} \tag{3}$$

Where, r and c are the row count and column count respectively.

I_{M2}: is the greenness index average calculated for the entire image given by Eq. 4.

$$I_{M2} = \frac{1}{rc\sum I(i,j)} \tag{4}$$

I_{M3} and I_{M4}: have the effect of segmenting comparable shades of green and substituting with mean given by Eq. 5. and Eq. 6. respectively.

$$I_{M3} = \frac{1}{N}\sum_{K=1}^{K}\sum_{i,j}^{n_k}\sqrt{I(i,j)I_{zk}(i,j)} \tag{5}$$

$$I_{M4} = \frac{1}{N}\sum_{K=1}^{K}\sum_{i,j}^{n_k}\frac{I(i,j)I_{zk}(i,j)}{2} \tag{6}$$

The final two methods (I_{M3}, I_{M4}) involve segmenting the image into K distinct regions (Z_k) based on color similarity. For each region, the characteristic index value (I_{zk}) is calculated. In these equations, I(i,j) is the greenness index value at pixel coordinates (i, j), I_{zk} is the characteristic index value for the segmented region Z_k to which the pixel belongs, N is the total number of pixels (N = r c) and n_k is the number of pixels within region Z_k.

Following the same convention, a further eight metrics from Kawashima's and Pagola's methodologies were designated with the unique identifiers ($I_{kaw}M_1$-$I_{kaw}M_4$, $I_{pca}M_1$-$I_{pca}M_4$).

Non-linear regression framework for N estimation

The relationship between these metric values and actual N content is non-linear. Therefore, a adapted logistic regression model (Eq. 7) was fitted for each metric to estimate N levels.

$$f(x) = \beta_1\left(\frac{1}{2} - \frac{1}{1+e^{\beta_2(x-\beta_3)}}\right) + \beta_4 x + \beta_5 \quad (7)$$

This formulation combines a logistic transformation with a linear adjustment, improving flexibility for capturing non-linear trends. The parameters $\beta_1, \beta_2, \beta_3, \beta_4$ were estimated using ground truth N measurements obtained *via* Kjeldahl digestion and Greenseeker. Model fitting was performed separately for each dataset and evaluated in terms of correlation with laboratory values.

Statistical analysis

A quantitative analysis was conducted to validate the efficacy of the proposed framework. The evaluation relied on a set of statistical metrics, the Pearson correlation coefficient (ρ), the Spearman rank correlation coefficient (r_s), the root mean square error (RMSE) and ANOVA test.

The Pearson coefficient (Eq. 8) measures the strength of the linear relationship between predicted (y) and observed (x) values, ranging from −1 to +1, where values close to ±1 indicate strong correlation.

$$\rho = \frac{\sum_i (x_i - \bar{x})(y_i - \bar{y})}{\sqrt{\sum_i (x_i - x)^2}\sqrt{\sum_i (y_i - \bar{y})^2}} \quad (8)$$

Where $\bar{\boldsymbol{x}}$ and $\bar{y}$ are the average of x and y.

The Spearman rank correlation (Eq. 9) evaluates monotonic relationships by comparing ranked values. It is particularly useful for non-linear associations and is defined as:

$$r_s = 1 - \frac{6\sum(x_i - y_i)^2}{n(n^2-1)} \quad (9)$$

Where n is the sample count.

Finally, the RMSE (Eq. 10) quantifies the average deviation between predicted and observed values. Lower RMSE values indicate higher predictive accuracy, with zero representing perfect agreement.

$$RMSE = \sqrt{\sum_{i=1}^{n}(y_i - \hat{y})^2} \quad (10)$$

Analysis of Variance (ANOVA) finds whether there are notable differences in results across two or more groups. There are various forms of ANOVA, parametric and non-parametric. In our case, it is advisable to apply non-parametric methods as there is a difference in the variance of groups. In this study, the PERMANOVA (Permutational Multivariate Analysis of Variance) (Anderson 2017) test is adopted that calculate $F_{statistic}$ (Eq. 11).

$$F_{statistic} = \frac{SS_{Between}/(k-1)}{SS_{Within}/(n-k)} \quad (11)$$

Where, k is number of groups, n is total number of observations $SS_{Between}$ is between group sum of squares, SS_{Within} is within group sum of squares.

Results

The application of the image-based pipeline yielded accurate estimates of N content, demonstrating its overall viability. This section details these findings, beginning with an overview of the model's aggregate performance across the diverse set of smartphones and varieties. Subsequently, the framework's generalizability is investigated through an examination of variety-specific estimation accuracy. Finally, the hypothesis that camera resolution has a negligible effect on metric stability is statistically tested using a PERMANOVA test.

Collective performance across devices and varieties

Metric M_9, defined as (G - B), demonstrated the strongest overall performance, achieving the highest correlation and lowest error in all three datasets (Table 3). For Dataset I, M_9 yielded values of ρ = 0.6537, r_s = 0.6587 and RMSE = 1.6845. It maintained robust performance in Datasets II (ρ = 0.5376, r_s = 0.5417, RMSE = 1.8944) and III (ρ = 0.5758, r_s = 0.5894, RMSE = 1.8338), indicating resilience to variations in camera resolution. Metric M_{16}, $\frac{2R(G-B)}{(G+B)}$, consistently ranked second across all datasets, suggesting that normalization by the red channel provides additional, though lesser, predictive utility.

Variety-specific performance for N estimation

Given the visible variation in leaf coloration among the 11 maize varieties (Fig. 6), a per-variety analysis was conducted. This approach yielded improved correlation scores compared to the collective analysis, underscoring the influence of varietal phenotypic traits on color-based estimation.

The top-performing metric varied by variety and, to a lesser extent, by dataset (Table 5). For example, the optimal metric for Sweet-1 was M_{15} in Dataset I and $I_{kaw}M4$ in Dataset II. Despite this variance, metrics M_9 and M_6 frequently appeared among the top performers across most varieties and datasets. Metric M_6 emerged as the most frequently optimal choice, ranking in the top three for the

Table 3: Comprehensive performance comparison color-based vegetation indices across three smartphone imaging datasets. The table presents Pearson correlation (r), Spearman correlation (ρ), and Root Mean Square Error (RMSE) values for each metric, with the best-performing result for each dataset and statistical measure highlighted in bold

Metric	Dataset I			Dataset II			Dataset III		
	ρ	r_s	RMSE	ρ	r_s	RMSE	ρ	r_s	RMSE
M_1	0.04	0.05	2.22	0.28	0.24	2.15	0.23	0.18	2.18
M_2	0.18	0.17	2.18	0.34	0.34	2.10	0.27	0.24	2.15
M_3	0.36	0.27	2.07	0.17	0.18	2.21	0.23	0.23	2.18
M_4	0.30	0.31	2.11	0.27	0.29	2.15	0.32	0.32	2.12
M_5	0.56	0.57	1.84	0.28	0.31	2.15	0.34	0.39	2.10
M_6	0.59	0.60	1.78	0.38	0.37	2.07	0.46	0.46	1.98
M_7	0.33	0.36	2.09	0.22	0.25	2.19	0.11	0.13	2.22
M_8	0.54	0.54	1.86	0.45	0.46	1.99	0.51	0.50	1.92
M_9	0.65	0.65	1.68	0.53	0.54	1.89	0.57	0.58	1.83
M_{10}	0.23	0.29	2.16	0.00	0.09	2.24	0.13	0.10	2.22
M_{11}	0.51	0.55	1.90	0.37	0.37	2.08	0.44	0.46	2.00
M_{12}	0.58	0.62	1.80	0.40	0.40	2.05	0.44	0.47	2.00
M_{13}	0.28	0.33	2.13	0.04	0.12	2.24	0.13	0.08	2.22
M_{14}	0.50	0.54	1.91	0.38	0.38	2.07	0.46	0.45	1.99
M_{15}	0.58	0.62	1.79	0.39	0.37	2.06	0.42	0.46	2.03
M_{16}	0.64	0.65	1.70	0.51	0.51	1.92	0.56	0.57	1.85
M_{17}	0.57	0.57	1.82	0.47	0.47	1.98	0.54	0.53	1.88
M_{18}	0.26	0.31	2.14	0.08	0.09	2.23	0.18	0.22	2.04
$I_{kaw}M_1$	0.51	0.55	1.90	0.42	0.41	2.03	0.49	0.51	1.94
$I_{kaw}M_2$	0.50	0.54	1.91	0.37	0.38	2.07	0.47	0.49	1.97
$I_{kaw}M_3$	0.51	0.55	1.90	0.38	0.38	2.07	0.45	0.47	1.99
$I_{kaw}M_4$	0.45	0.54	1.97	0.35	0.34	2.10	0.42	0.44	2.02
$I_{pca}M_1$	0.53	0.54	1.87	0.50	0.49	1.94	0.54	0.55	1.87
$I_{pca}M_2$	0.35	0.30	2.01	0.50	0.50	1.93	0.50	0.55	1.87
$I_{pca}M_3$	0.32	0.29	2.13	0.49	0.50	1.94	0.55	0.55	1.87
$I_{pca}M_4$	0.33	0.44	2.09	0.48	0.50	1.96	0.53	0.55	1.89

For systematic reference, each metric was assigned a unique identifier using "M" to denote "Metric" with numerical subscripts ranging from 1 to 18, Following the same convention, a further eight metrics from Kawashima's and Pagola's methodologies were designated with the unique identifiers ($I_{kaw}M_1$-$I_{kaw}M_4$, $I_{pca}M_1$-$I_{pca}M_4$)

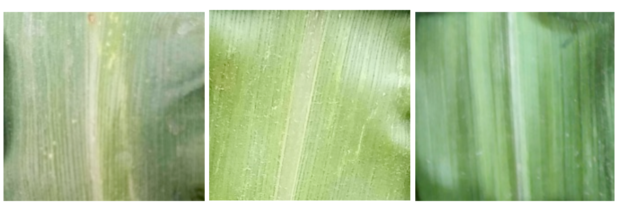

(a) (b) (c)

Fig. 6: Inter-variety leaf color variation under standardized imaging. Samples from a Samsung smartphone for (**a**) Gohar-19, (**b**) Fh-1046 and (**c**) Yh-548 highlight the distinct color profiles that correlate with nitrogen status, forming the basis for the variety wise colorimetric analysis

highest number of varieties, followed by M_9 and M_7 (Fig. 7). This consistency suggests that M_6 and M_9 capture fundamental color features strongly associated with N content, with effectiveness modulated by varietal characteristics.

PERMANOVA Test for camera resolution effect

PERMANOVA (Anderson 2017) was employed to test the null hypothesis using Algorithm 1. The following hypotheses were formulated:

- H_0: No significant difference exists among the three mobile phone groups for a given metric.
- H_1: At least one group mean significantly differs from the others.

The resulting *P*-values for most metrics were below the *0.05* significance threshold (Table 4), leading to a rejection of the null hypothesis. This indicates that camera resolution has a statistically significant effect on the values of the majority of color metrics. In contrast, the metrics based solely on the R or G channel did not show significant differences, suggesting they are less sensitive to imaging hardware. These results confirm that camera resolution is a critical parameter that must be controlled for or accounted for in the development of color-based N estimation models.

Algorithm 1: Permutation-based ANOVA using F-Statistic

Input
Require: X is a data matrix with n samples and p variables, g is a grouping variable with k groups, and N the permutations count Steps:

1. Calculate the overall mean of the data: $\bar{X} = \frac{1}{n}\sum_{i=1}^{n} X_i$
2. For each group j = 1, ..., k: $\bar{X} = \frac{1}{n_j}\sum_{i \epsilon g_j} X_i$
3. Compute the between-group sum of squares: $$SS_{between} = \sum_{j=1}^{k}(\bar{X}_j - \bar{X})^2$$
4. Compute the within-group sum of squares: $$SS_{within} = \sum_{j=1}^{k}\sum_{i \epsilon g_j}(\bar{X}_i - X_j)^2$$
5. Compute the observed F-statistic: $f_{obs} = \frac{SS_{between}/(k-1)}{SS_{within}/(n-k)}$
6. Initialize: P = 0
7. For i = 1 to N: a. Randomly permute the group labels g → g'; b. Recalculate the F-statistic F_i using g'; c. If $F_i \geq F_{obs}$ then P = P + 1
8. Compute the p-value: p = P / N
9. Return p

Discussion

This study established a pipeline for non-destructive N estimation in maize by integrating deep learning segmentation with the analysis of color-based metrics derived from smartphone imagery. The core finding, that the simple M_9 (G - B) metric demonstrated superior robustness across devices and varieties, aligns with previous work by Dey *et al*. (2016), who also found differentials between green and blue channels to be strongly associated with chlorophyll content. The consistent performance of metrics like M_6 and M_7 further suggests that ratios incorporating normalization (*e.g.*, by the red channel or sum of channels) enhance stability, a concept supported in various plant phenotyping contexts (Rigon *et al*. 2016; Mamta *et al*. 2024).

However, the observed varietal deviations in optimal metrics are a critical result. This indicates that a one-size-fits-all model is suboptimal. The color expression of N deficiency

Table 4: PERMANOVA results quantifying the influence of smartphone camera on color-based nitrogen indices. The analysis reveals that camera model had a significant effect ($P < 0.05$), supporting the framework's hardware invariance

Metric	F Statistic	*P* value	H_0
M_1	0.263	*0.7762*	Not Reject
M_2	0.612	*0.5634*	Not Reject
M_3	55.68	*0.0009*	Reject
M_4	60.12	*0.0009*	Reject
M_5	94.64	*0.0009*	Reject
M_6	130.3	*0.0009*	Reject
M_7	3629	*0.0009*	Reject
M_8	85.22	*0.0009*	Reject
M_9	73.30	*0.0009*	Reject
M_{10}	2596	*0.0009*	Reject
M_{11}	138.4	*0.0009*	Reject
M_{12}	135.4	*0.0009*	Reject
M_{13}	2451	*0.0009*	Reject
M_{14}	135.0	*0.0009*	Reject
M_{15}	133.6	*0.0009*	Reject
M_{16}	78.33	*0.0009*	Reject
M_{17}	94.84	*0.0009*	Reject
M_{18}	90.23	*0.0009*	Reject
$I_{kaw}M_1$	83.49	*0.0009*	Reject
$I_{kaw}M_2$	104.4	*0.0009*	Reject
$I_{kaw}M_3$	109.6	*0.0009*	Reject
$I_{kaw}M_4$	83.76	*0.0009*	Reject
$I_{pca}M_1$	383.0	*0.0009*	Reject
$I_{pca}M_2$	251.7	*0.0009*	Reject
$I_{pca}M_3$	221.4	*0.0009*	Reject
$I_{pca}M_4$	10.55	*0.0009*	Reject

For systematic reference, each metric was assigned a unique identifier using "M" to denote "Metric" with numerical subscripts ranging from 1 to 18, Following the same convention, a further eight metrics from Kawashima's and Pagola's methodologies were designated with the unique identifiers ($I_{kaw}M_1$-$I_{kaw}M_4$, $I_{pca}M_1$-$I_{pca}M_4$)

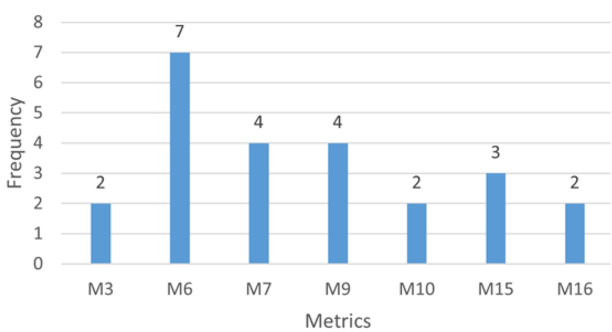

Fig. 7: Comparative distribution of top-performing metrics across genetic varieties. The bar chart illustrates the frequency with which each metric was ranked as a top-performer across the different genetic varieties analyzed. The numerical value at top of each bar indicates the specific count of varieties in which the corresponding metric achieved a top-ranking result. This visualization demonstrates that metric M_6 exhibits consistently high performance across the highest number of varieties, thereby supporting its reliability as a robust candidate for generalized nitrogen estimation models

Metrics: M_3: B, M_6:$\frac{B}{(R+G+B)}$, M_7:$R-G$, M_9:$G-B$, M_{10}:$\frac{(R-G)}{(R+G)}$, M_{15}:$\frac{(G-B)}{(R+G+B)}$, M_{16}:$\frac{2R(G-B)}{(G+B)}$

is mediated by genotypic differences in leaf pigmentation and structure, a factor often overlooked in broader phenotyping studies (Buchaillot *et al.* 2019). Consequently, for maximum accuracy, calibration should be variety-specific, or models must be trained on diverse genetic material to capture this heterogeneity. A pivotal insight from our analysis is the statistically significant effect of camera resolution on metric values, as confirmed by the PERMANOVA results (Anderson 2017). This underscores a major practical consideration for field deployment: an estimation model developed on images from one sensor cannot be directly ported to another without risking significant error. This finding challenges the assumption that standard RGB metrics are inherently device-agnostic and emphasizes the need for resolution-aware calibration or sensor standardization in future frameworks. Positioning our work within the existing technological landscape highlights its specific contributions. Compared to high-accuracy CNN methods (Sun *et al.* 2024) our approach offers greater interpretability and explicitly addresses hardware variance. While vision-based indices like GCV are effective (Haider *et al.* 2021), their validation is often limited to controlled conditions, unlike our field-based imagery. Advanced platforms like robotic under-canopy imagers (Bestas *et al.* 2025) or UAVs with multispectral sensors (Osco *et al.* 2020) provide unparalleled data quality but remain cost-prohibitive. Our methodology achieves a favorable compromise, leveraging ubiquitous smartphones to deliver comparable accuracy at a fraction of the cost, thus enhancing accessibility.

Unlike large-scale phenotyping efforts that provide insights at the genotype level (Buchaillot *et al.* 2019), this pipeline establishes a foundation for assessing N status at a finer spatial resolution. The release of our large, annotated dataset supports further development in this area.

While the proposed framework demonstrates robust N estimation under the tested conditions, but there are some limitations as well. The model's performance remains susceptible to extreme variations in natural light, such as intense shadows or specular highlights, which can alter color perception. Furthermore, the reliance on clear, top-down leaf images means that highly oblique orientations or significant leaf curling were not fully accounted for in the current analysis. Future research will therefore focus on integrating advanced color constancy algorithms to neutralize lighting effects and developing model's invariant to handle leaf angle along with investigation for more hardware calibrations (camera resolutions).

Conclusion

This study establishes a smartphone-based computer vision framework that accurately estimates maize leaf N content using standard RGB imagery. The method achieved strong agreement with laboratory measurements, with specific color metrics M6, M9 and M7 identified as robust predictors across and within varieties. A critical finding is that camera sensor specifications significantly influence color metrics, underscoring the need for sensor-aware models to ensure cross-device reliability. Along with model a comprehensive,

Table 5: Top-performing vegetation indices and their statistical performance across eleven maize varieties and three imaging datasets. For each variety-dataset combination, the table identifies the optimal metric from (M_1–M_{18}, $I_{kaw}M_1$–$I_{kaw}M4$ and $I_{pca}M1$-$I_{pca}M4$) alongside its corresponding Pearson correlation (ρ), Spearman correlation (r_s) and Root Mean Square Error (RMSE) values, demonstrating the context-dependent nature of metric performance for nitrogen estimation

Variety	Dataset I				Dataset II				Dataset III			
	Metric	ρ	r_s	RMSE	Metric	ρ	r_s	RMSE	Metric	ρ	r_s	RMSE
Sahiwal Gold	M_6	0.75	0.60	0.95	M_{15}	0.76	0.77	0.92	M_6	0.83	0.81	0.78
CIMMYT PAK	M_6	0.87	0.81	1.11	M_7	0.87	0.82	1.13	M_{15}	0.77	0.83	1.49
Agaiti-72	M_6	0.94	0.67	0.67	M_2	0.78	0.63	1.31	$I_{pca}M_1$	0.88	0.82	0.97
Akbar	M_{15}	0.91	0.93	0.87	M_7	0.79	0.69	1.36	M_6	0.82	0.75	1.27
Pop-1	M_{10}	0.22	0.79	0.53	M_1	0.75	0.79	0.93	$I_{pca}M_2$	0.63	0.51	1.57
Sweet-1	M_5	0.84	0.75	1.06	$I_{kaw}M_4$	0.78	0.80	1.18	M_{17}	0.87	0.86	0.91
Gohar-19	M_3	0.93	0.78	0.62	M_6	0.80	0.87	0.86	M_{16}	0.89	0.82	0.76
Yh-1898	M_9	0.93	0.87	0.62	$I_{pca}M_3$	0.94	0.83	0.73	M_6	0.72	0.65	1.48
Fh-1046	M_7	0.74	0.77	1.81	$I_{pca}M_1$	0.75	0.73	1.78	M_7	0.72	0.62	1.64
Yh-548	M_8	0.92	0.85	0.85	M_{14}	0.77	0.76	1.31	M_6	0.73	0.55	1.41
Yh-5427	M_6	0.60	0.47	2.32	M_1	0.92	0.66	1.24	M_2	0.97	0.58	0.69

[6]For systematic reference, each metric was assigned a unique identifier using "M" to denote "Metric" with numerical subscripts ranging from 1 to 18, Following the same convention, a further eight metrics from Kawashima's and Pagola's methodologies were designated with the unique identifiers ($I_{kaw}M_1$-$I_{kaw}M_4$, $I_{pca}M_1$-$I_{pca}M_4$)

multi-variety dataset was compiled under controlled N treatments. Future work will focus on expanding the model's applicability to other staple cereals like wheat and rice while improving its resilience to real-world variables including dark light conditions and varied leaf angles.

Acknowledgments

The authors would like to thank Dr. Amjad Khan, Senior Scientist at Maize & Millets Research Institute, Yusafwala, Sahiwal and Dr. Muhammad Faisal, Assistant Professor (then) at Department of Soil Science, University of the Punjab, Lahore for their assistance in data collection.

Author Contribution

Conceptualization: MSF and RZ; Methodology: MSF, RZ and MHK; Software: MSF, RZ and MHK; Writing-original draft preparation was done by MSF and RZ; Writing-review and editing by MSF, RZ and RM; Supervision by MSF, RM and MHK; Project administration, MSF, RZ and MHK; Funding acquisition: MSF and RM. All authors were involved validation, formal analysis, investigation, resources and data curation.

Conflicts of Interest

The authors declare that they have no conflict of interest.

Data Availability

The dataset is publicly available at the project website.

Ethics Approval

Not applicable to this paper.

Funding Source

This research was partially supported by a research grant (No. 21-140) from Punjab Agricultural Research Board (PARB), Pakistan.

References

Adhikari R, C Li, K Kalbaugh, K Nemali (2020). A low-cost smartphone controlled sensor based on image analysis for estimating whole-plant tissue nitrogen (N) content in floriculture crops. *Comput Electr Agric* 169:105–173

Agarwal A, SD Gupta (2018). Assessment of spinach seedling health status and chlorophyll content by multivariate data analysis and multiple linear regression of leaf image features. *Comput Electr Agric* 152:281–289

Altuntaş Y, E Elkoca, S Kodaz (2024). Impact of Mesorhizobium ciceri inoculation on symbiotic nitrogen fixation of various chickpea (*Cicer arietinum* L.) cultivars. *J Agric Prod* 5:255–264

Amaral ESD, DV Silva, LD Anjos, AC Schilling, ÂC Dalmolin, MS Mielke (2018). Relationships between reflectance and absorbance chlorophyll indices with RGB (Red, Green, Blue) image components in seedlings of tropical tree species at nursery stage. *New For* 50:377–388

Anderson MJ (2017). Permutational multivariate analysis of variance (PERMANOVA). *In: Wiley StatsRef: Statistics Reference Online*, pp:1–15. John Wiley & Sons

Bestas Z, HMV Es, WD Philpot, KC Bares, DG Rossiter (2025). High-resolution sensing of maize nitrogen status through under-canopy RGB imaging using a mobile platform. *Precis Agric* 26:1-30

Buchaillot ML, AG Romero, OV Diaz, MA Zaman-ullah, A Tarekegne, JE Cairns, BM Parsanna, JL Araus, SC Kefauver (2019). Evaluating maize genotype performance under low nitrogen conditions using RGB UAV phenotyping techniques. *Sensors* 19:1-27

Chen B, X Lu, S Yu, S Gu, G Huang, X Guo, C Zhao (2022). The application of machine learning models based on leaf spectral reflectance for estimating the nitrogen nutrient index in maize. *Agriculture* 12:1-18

Chen Z, F Wang, P Zhang, C Ke, Y Zhu, W Cao, H Jiang (2020). Skewed distribution of leaf color RGB model and application of skewed parameters in leaf color description model. *Plant Meth* 16:1-8

Colorado JD, NC Bornacelli, JS Caldas, E Petro, MC Rebolledo, D Cuellar, F Calderon, IF Mondragon, AJ Botero (2020). Estimation of nitrogen in rice crops from UAV-captured images. *Remote Sens* 12:1-31

Dey AK, M Sharma, MR Meshram (2016). An analysis of leaf chlorophyll measurement method using chlorophyll meter and image processing technique. *Proc Comput Sci* 85:286–292

Ghazal S, A Munir, WS Qureshi (2024). Computer vision in smart agriculture and precision farming: techniques and applications. *Comput Electr Agric* 202:107313

Govindasamy P, SK Muthusamy, M Bagavathiannan, J Mowrer, PTK Jagannadham, A Maity, HM Halli, GK Sujayanand, R Vadivel, TK Das, R Raj, V Pooniya, S Babu, SS Rathore, L Murlikrishnan, G Tewari (2023). Nitrogen use efficiency—a key to enhance crop productivity under a changing climate. *Front Plant Sci* 14:1-19

Gürbüz MA, TA Kardeş (2024). Sunflower-nitrogen calibration based on the amount of mineral nitrogen in soil under rainfed conditions in Thrace region. *Soil Stud* 13:43–54

Haider T, MS Farid, R Mahmood, A Ilyas, MH Khan, STA Haider, MH Chaudhry, M Gul (2021). A computer-vision-based approach for nitrogen content estimation in plant leaves. *Agriculture* 11:1-19

Kamilaris A, FX Prenafeta-Boldú (2018). Deep learning in agriculture: A survey. *Comput Electr Agric* 147:70–90

Kawashima S, M Nakatani (1998). An algorithm for estimating chlorophyll content in leaves using a video camera. *Ann Bot* 81:49–54

Kulkarni N (2012). Color thresholding method for image segmentation of natural images. *Intl J Image Graph Signal Proc* 4:25–31

Lu B, PD Dao, J Liu, Y He, J Shang (2020). Recent advances of hyperspectral imaging technology and applications in agriculture. *Remote Sens* 12:1-44

Mamta K, Suman, D Prasad (2024). Crop yield prediction using remote sensing: A review. *In: 2024 International Conference on Computational Intelligence and Computing Applications (ICCICA)*, Vol. 1, pp:547–552. IEEE

Osco LP, JM Junior, APM Ramos, DEG Furuya, DC Santana, LPR Teodoro, WN Gonçalves, FHR Baio, H Pistori, CAdS Junior, PE Teodoro (2020). Leaf nitrogen concentration and plant height prediction for maize using UAV-based multispectral imagery and machine learning techniques. *Remote Sens* 12:1-17

Pagola M, R Ortiz, I Irigoyen, H Bustince, E Barrenechea, PA Tejo, C Lamsfus, B Lasa (2009). New method to assess barley nitrogen nutrition status based on image colour analysis: comparison with SPAD-502. *Comput Electr Agric* 65:213–218

Qin X, Z Zhang, C Huang, M Dehghan, OR Zaiane, M Jagersand (2020). U2-Net: going deeper with nested U-structure for salient object detection. *Pattern Recogn* 106:1-15

Rawal N, KR Pande, R Shrestha, SP Vista (2022). Nutrient use efficiency (NUE) of wheat (*Triticum aestivum* L.) as affected by NPK fertilization. *PLoS One* 17:1–19

Rigon JPG, S Capuani, DM Fernandes, TM Guimarães (2016). A novel method for the estimation of soybean chlorophyll content using a smartphone and image analysis. *Photosynthetica* 54:559–566

Sánchez-Sastre LF, NMSAD Veiga, NM Ruiz-Potosme, P Carrión-Prieto, JL Marcos-Robles, LM Navas-Gracia, P Martín-Ramos (2020). Assessment of RGB vegetation indices to estimate chlorophyll content in sugar beet leaves in the final cultivation stage. *Agri Eng* 2:128–149

Shafarenko L, M Petrou, J Kittler (1997). Automatic watershed segmentation of randomly textured color images. *IEEE Trans Image Process* 6:1530–1544

Sun L, C Yang, J Wang, X Cui, X Suo, X Fan, P Ji, L Gao, Y Zhang (2024). Automatic modeling prediction method of nitrogen content in maize leaves based on machine vision and CNN. *Agron* 14:1-15

Sun Y, CK Tang, YW Tai (2021). Semantic image matting. *In: Proceedings of the IEEE/CVF Conference on Computer Vision and Pattern Recognition,* pp:11120–11129

Taheri F, A Maleki, A Fathi (2021). Study of different levels of nitrogen fertilizer and irrigation on quantitative and qualitative characteristics of Quinoa grain yield. *Crop Physiol J* 13:135–149

Yang H, B Ming, C Nie, B Xu, J Xin, X Lu, J Xue, P Hou, R Xie, K Wang, S Li (2022). Maize canopy and leaf chlorophyll content assessment from leaf spectral reflectance: Estimation and uncertainty analysis across growth stages and vertical distribution. *Remote Sens* 14:1-22

Yang Z, P Willis, R Mueller (2008). Impact of band-ratio enhanced AWIFS image on crop classification accuracy. *In: Proceedings of the Pecora,* Vol. 17, pp:1-11. Going Operational, Denver, CO, USA

Yokamo S, M Irfan, W Huan, B Wang, Y Wang, M Ishaq, D Lu, X Chen, Q Cia, H Wang (2023). Global evaluation of key factors influencing nitrogen fertilization efficiency in wheat: a recent meta-analysis (2000-2022). *Front Plant Sci* 14:1-17